

Modelling and Analysis of Dynamic Frictional Interactions of Vibro-Driven Capsule Systems with Viscoelastic Property

Pengcheng Liu¹ · Hongnian Yu^{2,4*} · Shuang Cang³

*Corresponding Author: yu61150@ieee.org

Abstract

This paper studies the dynamic frictional interactions of the underactuated vibro-driven capsule systems with the viscoelastic property. Frictional dynamics of the capsule systems is an active research domain, while the online implementation and control of the friction models are still intractable tasks. This paper investigates the frictional characteristics of the capsule systems in the dynamic regime, including particularly the non-reversible drooping and hysteresis. Firstly, the frictional interaction dynamics is modelled and characterized using a combined physics-based and analytical-based approach. Subsequently, the qualitative changes in the capsule dynamics and friction-induced vibrational responses that triggered by multiple control parameters are discussed. It is found that the capsule dynamics is mainly periodic, and the motion velocity of the capsule systems can be controlled by appropriate tuning of the control parameters around the identified control points. Simulation results have a good agreement with the experimentally observed frictional characteristics. The effectiveness of the proposed method is verified in terms of satisfaction of the energy requirements and quenching of the friction-induced vibrations. It is also found that the frictional interaction dynamics of the capsule systems can be predicted for a wide range of vibrational behaviours. Finally, the importance of a concrete understanding and accurate description of the dynamic friction at the sliding substrate is highlighted.

Keywords

Vibro-driven dynamics; Underactuated system; Capsule systems; Friction and hysteresis; Viscoelasticity

1. Introduction

During the past decade, autonomous micro-mechanical systems have become an active research topic in both robotics and control communities. Various systems have been studied, for instance, the rigid body with two internal masses (Bolotnik and Figurina, 2008), the two-body system (Chernous'ko, 2011), the capsulobot (Huda and Yu, 2015a; Liu et al., 2018a, 2018b), the vibro-impact capsule systems (Liu et al., 2018c, 2017; Zhan and Xu, 2015; Zhang et al., 2014a). These systems move by generating the internal autogenetic forces and overcoming the external environmental resistance. Equipped with hermetic structure and smooth surface, they have extensive applications, for instance, in engineering

¹ Lincoln Centre for Autonomous Systems (L-CAS), University of Lincoln, Lincoln LN6 7TS, United Kingdom

² School of Computer Science and Network Security, Dongguan University of Technology, Dongguan 523808, China

³ Newcastle Business School, Northumbria University, Newcastle NE1 8ST, UK

⁴ Faculty of Science and Technology, Bournemouth University, Poole BH12 5BB, United Kingdom

diagnosis, medical endoscopy, disaster rescues and seabed exploration. Irrespective of the complex gear case and external protruding components, they are simple in mechanical structure and prone to control, which shed light on the design of the dynamical model of autonomous and bionic-robotic systems. The rectilinear locomotion is based on the principle that an internal vibro-driven mass moves and interacts with the system body and overcomes the environmental resistant forces. Capsule systems are designed with this principle to work in vulnerable media and restricted space, for instance, minimally invasive diagnosis inside a human body and pipeline inspection into a narrow tube. The dynamics of a mobile system with an internal acceleration-controlled mass based on the stick-slip effect was studied in (H. Fang and Xu, 2011). The issue of trajectory tracking control of an underactuated capsulobot system was studied in (Huda and Yu, 2015), which proposed a two-stage motion control strategy through acceleration profiles. A vibro-driven capsule system was proposed in (Liu et al., 2014, 2016) and the issues of motion generation and dynamic interactions with the environment were studied. The capsule systems require high fidelity, which makes precise modelling and prediction of the frictional interactions is a nontrivial but intractable task. Conventionally, friction is considered as an instable factor that needs to be eliminated or compensated through the design of control systems. Robust friction models are required in some practical engineering problems. However, friction plays a pivotal role in the locomotion of the self-propelled capsule systems. For the vibro-driven system considered in this paper, the dynamic coupling between the driving mechanism and the capsule are utilized to generate desirable stick-slip motions. Hence, accurate predictions of the dynamic interactions in the sticking, presliding and pure sliding regimes become crucial.

Various friction models have been proposed in the literature through investigation in the physical phenomena. These models have different numbers of parameters to be identified and controlled. Basically, there are three indexes (Al-Bender and Swevers, 2008) for evaluating the friction model: 1) simple for online utilization; 2) sophisticated to describe all frictional characteristics; and 3) having a limited number of parameters to be identified. As a simplified friction model, the Coulomb model describes the friction as a function of relative velocity between two bodies in contact (Armstrong-Hélouvy et al., 1994), and it has been widely used for studying capsule systems such as in (Chernous'ko, 2002; Fang and Xu, 2011; Huda and Yu, 2015; Li et al., 2006; Liu et al., 2013b). Some significant studies on stick-slip motions of a single-module vibro-driven motion system have been reported in (Fang and Xu, 2013; H. B. Fang, 2010). Towards a capsule endoscope inside an intestine, an analytical frictional resistance model was studied in (Kim et al., 2007), the contact geometry and viscoelasticity of the lubricants on the intestine surface was considered to reveal the intestine characteristics, e.g., stress relaxation that results in lower frictional force with a decreasing capsule speed. Coulomb frictions, viscous friction and viscoelastic deformation of the intestinal wall were used in (Zhang et al., 2012) to study a capsule system inside an intestine, and the experiment results verified the friction model then the robot moves with a lower speed at $20\text{mm}\cdot\text{s}^{-1}$. These findings reveal that the low-speed stick-slip locomotion is a plausible motion pattern for the capsule system, and the friction characteristics are dominated by the intestine's villus-like structure and viscoelasticity. However, for specific applications

of the capsule systems, an accurate representation of the dynamic frictional interaction is required to capture several dynamic phenomena that have been observed in the experiments. Nevertheless, the static friction models solely consider the variations in velocities between the two bodies in frictional contact, while the hysteretic loops and the drooping frictional characteristics in the regime with lower relative velocity are not captured. Therefore, this paper models and analyses the dynamic interactions through the dominating components of the friction, including the static friction, presliding, breakaway force, stick-slip motion, the Stibbeck effect, friction memory and the hysteretic effect.

The drooping characteristic arises with dynamic frictional contact, and it is typically represented as a function of the relative velocity of the bodies in contact. In this regard, the friction is a single-valued function, which means it is driven by the reversible drooping to follow the same path in the deceleration stage (DS) and the acceleration stage (AS). However, the experimental observations are not always aligned with the consideration above, particularly in the unsteady environmental conditions such as the oscillations in relative velocity. Therefore, some engineering investigations have revealed that the frictional dynamics can be multi-valued, which means the friction force travels along different paths during the DS and the AS, and forms a non-reversible curve as reported in (Becker and Mahin, 2013; Biswas and Chatterjee, 2014; Neis et al., 2011; Outirba and Hendrick, 2014; Stefański et al., 2006; Wojewoda et al., 2008). The main reason for this phenomenon is the temporal lag between the variations of the friction force and the relative velocity. In the literature, both the clockwise (i.e. the friction force for the AS is greater than that for the DS) and the anticlockwise drooping loops have been observed in the pure sliding regime in engineering applications. Moreover, the hysteretic loops have been experimentally observed in the presliding regime based on the compliance property between the asperities induced by the spring-like behaviour as described in (Casini et al., 2012; Giannini et al., 2011). As a result, there is velocity overshooting during the initiation of stick-slip motion between the bodies in contact.

Single-degree-of-freedom (DOF) mass-spring-damper systems resting on a moving belt are well-adopted in literature to explore the friction-induced vibrations and experimentally observed friction characteristics (Hetzler et al., 2007; Saha et al., 2015). A majority of researches study on 2-DOF tangential-wise (typically linearly along the motion direction) vibrations as reported in (H. B. Fang and Xu, 2011; Huda and Yu, 2015; Liu et al., 2013b; Zhan and Xu, 2015) or the norm-wise vibrations as presented in (Chowdhury and Helali, 2008) w.r.t. the substrates in contact. These works form the main concept for self-propelled micro-robotic systems. However, the combined (nonlinear) norm-wise and tangential-wise vibrations that could generate bidirectional locomotion which has not been widely reported in the literature. It sheds light on a generalized significance for the studies on capsule systems. It is also noted that towards the nonlinear friction, there are several seminal studies in the literature (H. Fang and Xu, 2011; Fang and Xu, 2012). These works mainly focused on the qualitative changes induced by the control parameters with different friction models.

This paper considers the capsule systems which utilize combined tangential-wise and norm-wise vibrations to generate the underactuated locomotion. The nonlinear connection of the pendulum and the

vibrational actuator is characterized via a torsional spring and a viscous damper. Viscoelastic property is a promising feature for bio-inspired and soft robots, which enables efficient locomotion through natural oscillations. Many animals are capable of considerably reducing their metabolic cost of running through efficient utilization of the viscoelastic properties of muscles, tendons, and bones distributed in their bodies (Alexander et al., 1985) and limbs (Dimery et al., 1986; McMahon, 1985). The study on the relations between viscoelastic parameters and the system performance is beyond the scope of the work here and will be reported in due course. Motivated by the experimental findings in the literature, this paper studies the frictional forces described by the LuGre model (De Wit et al., 1995) (LM) and the Exponential model (Armstrong-Hélouvy et al., 1994) (EM). In the literature, only few works have reported the dynamic frictional interactions between the capsule system and the substrate. Towards this end, the non-reversible frictional characteristics (e.g., drooping and hysteresis) are studied. The dynamic interactions are firstly modelled using a combined physics-based and analytical-based approach. Then, this paper identifies the frictional limits for the static friction, the presliding regime and the pure sliding regime. Dynamic analysis of the friction-induced vibrational responses is then conducted, and the qualitative variations laws induced by the control parameter are identified. The analytical and numerical results have good agreements with the seminal findings in the literature. The proposed work is an advisable benchmark to exploit the challenges in friction compensation and online control of underactuated micro-robotic systems. The rest of the paper is organized as follows. The mathematical modelling of the capsule system and frictional interactions are provided in Section 2. Analysis of dynamic frictional interactions is presented in Section 3. Finally, conclusions are outlined in Section 4.

2. Mathematical modelling

2.1 System description

The 2-DOF capsule model is considered as shown in Fig. 1, which contains a pendulum and a platform merged with a rigid massless capsule shell. A vibration actuator is mounted on the platform at the pivot and connected with the pendulum. The movable pendulum is linked with the capsule body, and it is driven by a prescribed and harmonically excited force generated by the actuator. The actuator model is simplified here, and the interconnection between the pendulum and the capsule is represented by a torsional spring and a viscous damper. l and m are the length and mass of the pendulum, M is the mass of the platform. x and θ denote the absolute displacements of the capsule and the driving pendulum. k and c represent the coefficients of the stiffness and damping, respectively. It is assumed that the sliding friction force F_c between the capsule and the substrate is applied along the X-axis.

The motion principle of the capsule system is based on the interactions between the centripetal forces excited by the vibration actuator and the friction forces at the substrate. The system is propelled over a surface rectilinearly through the interactions with the friction. Elastic potential energy is accumulated and released in accordance with the contraction and relaxation of the torsional spring. The rotating pendulum drives the capsule to move bidirectionally via the dynamic couplings. The capsule motion begins with a static state, and it starts to move when the resultant force applied horizontally exceed the

threshold of the static friction at the surface in contact. The sticking phase dominates the system when the threshold is not reached. And once the condition is met, the capsule starts to move with the fast motion, which is termed as the pure sliding phase. The capsule model is developed to exploit advisable friction control approaches through the stick-slip effects. As a result, optimal forward motions can be generated, in which the capsule and the driving pendulum synchronize their motions harmoniously.

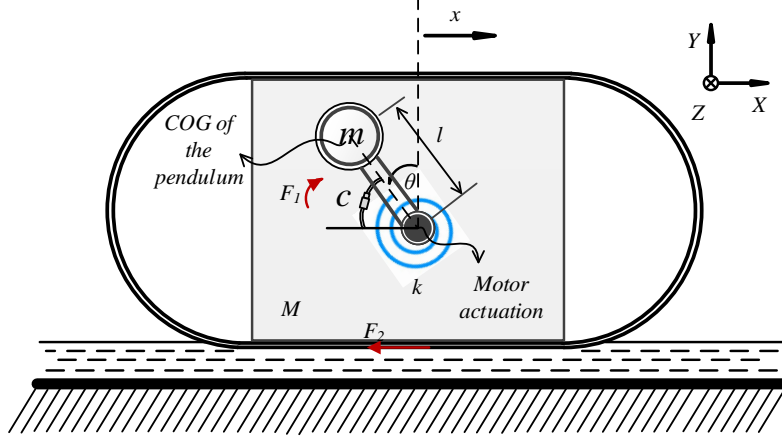


Fig.1. Schematic of the vibro-driven underactuated encapsulated system.

2.2 Dynamic model

Let the centre of the platform be the origin of the coordinate, x_b and y_b denote the absolute displacements measuring the deflection of the geometric centre of the ball referenced from the medial axis in horizontal and vertical direction, respectively. The configuration of the ball and its derivative are obtained as $x_b = x - l\sin(\theta)$, $y_b = l\cos(\theta)$, $\dot{x}_b = \dot{x} - l\dot{\theta}\cos(\theta)$ and $\dot{y}_b = -l\dot{\theta}\sin(\theta)$. Using the Euler-Lagrange's method, dynamics of the capsule system excited by harmonic force are described as

$$\frac{d}{dt} \frac{\partial L(q_i, \dot{q}_i)}{\partial \dot{q}_i} - \frac{\partial L(q_i, \dot{q}_i)}{\partial q_i} + F_i = Q_i \quad i = 1, 2. \quad (1)$$

where q_1 and q_2 denote the angular position θ and capsule displacement x , $L(q_i, \dot{q}_i) = E(q_i, \dot{q}_i) - V(q_i)$ is the Lagrangian function, E and V denote the kinetic energy and potential energy, F_i describes the friction and resistant forces, Q_i is the generalized externally applied force or moment. Details of the variables above are listed as follows: $E = \frac{1}{2}M\dot{x}^2 + \frac{1}{2}m\left[\left(\dot{x} - l\dot{\theta}\cos(\theta)\right)^2 + \left(-l\dot{\theta}\sin(\theta)\right)^2\right]$, $V = \frac{1}{2}k\theta^2 + mgl\cos(\theta)$, and $Q_1 = A\cos(\Omega t)$. It is noted that $F_1 = c\dot{\theta}$ denotes the viscous friction induced by the actuator, $F_2 = N_0F$ is the friction force between bodies in contact (with N_0 denoting the normal load and F describing the friction force per normal load unit). A and Ω are the amplitude and frequency of the harmonic force. g is the gravitational acceleration. Therefore, the equations of motion are derived as

$$ml^2\ddot{\theta} - ml\cos(\theta)\ddot{x} - mgl\sin(\theta) + k\theta + c\dot{\theta} = A\cos(\Omega t) \quad (2)$$

$$-ml\cos(\theta)\ddot{\theta} + (M + m)\ddot{x} + ml\sin(\theta)\dot{\theta}^2 + N_0F = 0 \quad (3)$$

We introduce a characteristic time scale using natural frequency $\omega_n = \sqrt{g/l}$ and a characteristic

length $x_0 = g/\omega_n^2$, the following non-dimensional motions of the equation are given as

$$\theta'' - \cos(\theta)X'' - \sin(\theta) + \rho\theta + v\theta' = h\cos(\omega\tau) \quad (4)$$

$$-\cos(\theta)\theta'' + (\lambda + 1) X'' + \sin(\theta)\theta'^2 + Nf = 0 \quad (5)$$

where θ and X represent the configuration variables with respect to θ and x in the non-dimensional space. Accordingly, the non-dimensional quantities are defined as

$$X = x/x_0, \lambda = M/m, \rho = k/(m l^2 \omega_n^2), \\ v = c/(m l^2 \omega_n), h = A/(m l^2 \omega_n^2), \omega = \Omega/\omega_n, N = N_0/(m l \omega_n^2)$$

It is noted that the prime (') in the equations above represents the derivatives in non-dimensionalized space $\tau = \omega_n t$, and f in Eq. (5) denotes the friction force under the non-dimensionalized relative velocity of the surfaces in contact.

Remark 1: In the normalized coordinate, the physical meanings of the control parameters can be captured as follows: λ represents the mass ratio, ρ and v respectively denote the dimensionless spring and damping coefficients, h and ω are dimensionless excitation amplitude and frequency.

2.3 Modelling and characterization of friction force dynamics

2.3.1 The physics-based analysis

Typically, friction arises at the physical interface between the contacting surfaces of different bodies in relative motions. It is assumed that the substrate is composed of a great number of tiny contacts on the surface irregularities, and the limit for a spring-like microscopic part of the contacting area is far larger than that for the bulk object. It can be concluded that the surfaces may have relative motion within a sufficiently small distance and without destroying the transitory connections. Also, the stretched irregularities gradually exert the elastic force to predominate the resisting friction force. It is noted that the above conclusion has different forms of interpretation, which is governed by the relative velocity between the bodies in contact. The reason behind is that the bonds may remain undisrupted for a period. The duration of the period is equivalent to the maximum extension of the micro-connections divided by the average velocity (McMillan, 1997). For the velocity near zero, the hysteretic effect may appear from the tiny movement between the two bodies in the phase of sticking, which is also named as micro-slip. The increasing number of connections being disrupted during a period can be associated with an increased friction force at a sufficiently fast average velocity. Hence, characteristics of the nonlinearity near zero relative velocities are the most significant to introduce the hysteretic effect. This is originated from the random distribution and size of asperities between the bodies in contact.

The capsule model rests on the horizontal plane, as shown in Fig. 2, and it is driven by a pendulum relative to the substrate with a velocity of $X'(\tau)$. For a small driving force in the horizontal direction, it is noted that the interface between the capsule and the surface falls into the sticking regime as shown in Fig. 2(a). As such, the stiction force results from the tension in conjoint irregularities. The brush-like surface illustration represents the evolution of the junction deflections between different asperities, and the tension on these connections. Nevertheless, as the driving force increases, the capsule moves with the displacement farther than the maximum extension of the connections. From Fig. 2(a), the capsule is initially stationary, and the connections are un-tensioned with no friction torque resisting the motion. In

Fig. 2(b), after a short period of time under the anticlockwise motion of the pendulum, the relative velocity of the capsule is appeared to be slightly positive, and the bonds remain intactness. The threshold will be met during the sticking phase via opposing torque of the friction force. At this critical boundary as depicted in Fig. 2(c), the capsule starts to slip with a kinematic friction force, which is characterized by a dramatic decrease. The clockwise motion of the pendulum results into a deceleration of the capsule to a slightly positive velocity, while it keeps slipping as the bonds need some time to reform (see Fig. 2(d)). The connections are re-built and the sticking phase arrives again when the capsule decelerates through $X'(\tau) = 0$ as shown in Figs. 2(e) and (f). Backward motions of the capsule follow the argument through Figs. 2(g) to (j). Following the discussions above, Fig. 3 shows the curve of friction force as a function of the average velocity of the capsule system. It is noted that the sketches in Fig.2 illustrate the motions of the capsule system to show the process and transition of sticking, presliding and sliding motion phases, which serves merely as an aid to intuition, please refer to (Liu et al., 2015) for detailed motion generation description.

The arguments above considers that the friction force depends solely on the relative velocity of the two bodies in contact (Armstrong-Hélouvry et al., 1994), i.e. $f(\tau) = f(X'(\tau))$, which gives rise to the reversible characteristic of the friction force (black solid line) as shown in Fig. 3. The capsule slips back onto a lately travelled trajectory where new asperities might have been reformed. The reason behind is that a unique value is generated for a given relative velocity during the DS and the AS. For dynamic frictional circumstance, however, it is necessary to take into account the state variable(s) associated with the average velocity $X'(\tau)$. The state variable may have different values for one particular relative velocity during the AS and the DS since they evolve with time by the description of differential equations. The arrows in green depict the different acceleration and deceleration paths that the capsule follows, and accordingly, a clockwise hysteretic loop is characterised in the pure sliding regime.

Remark 2: The phenomenon described above introduces the non-reversible characteristic of the friction force, which is demonstrated by different friction values during the AS and the DS (blue dashed line in Fig. 3). Therefore, the friction-velocity curve follows different paths for the AS and the DS, which gives rise to the hysteretic loops. For example, the non-reversible friction characteristic for the forced vibrations as shown in Fig. 3. This study aims to fill in the research gaps in modelling and analysing the dynamic interactions between the mobile capsule systems and the substrate.

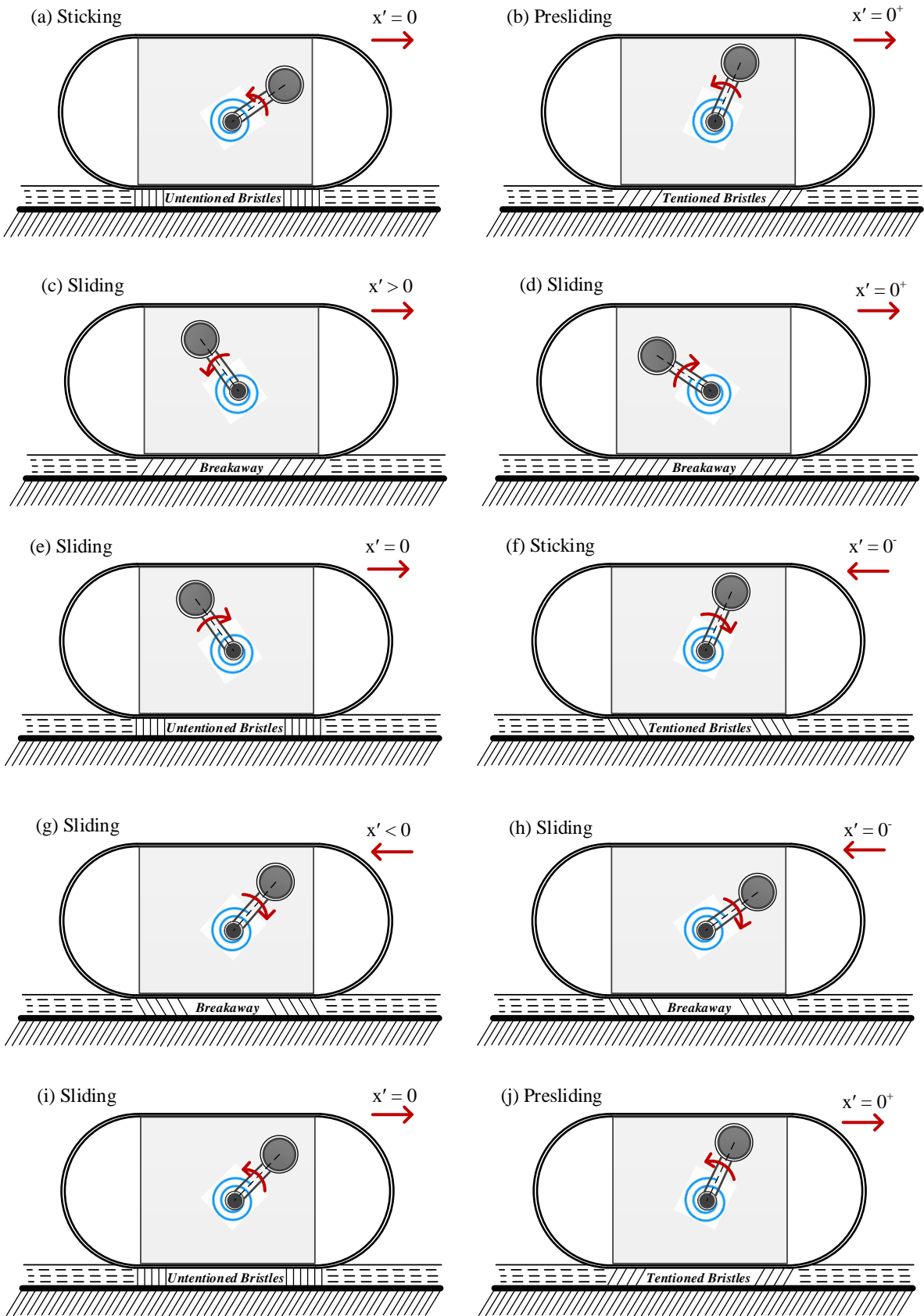


Fig.2. Schematic of the capsule motions with interface deformation.

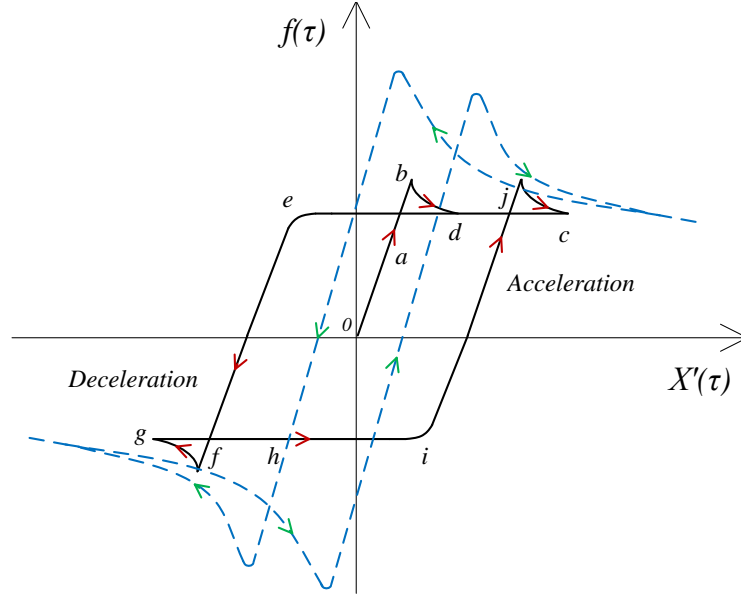


Fig.3. Schematic of the reversible (black solid line) and non-reversible (blue dashed line) characteristics of the friction forces.

2.3.2 Friction models

Two friction models (the LM and the EM) are employed as the first approximations to describe the tribological interactions between the capsule and the locomotion substrate in the tangential direction. Surface asperities are used in the LM to model the damped spring-like bristles between the bodies in contact. As a result, the micro-slip during the small displacement (the presliding) and the Sticbeck effect in massive displacement (the pure sliding) are revealed in the model. The external environmental force governs the bristles' deformation and reformation. As a result, the friction force is determined by a linear viscous term and the resultant deflection of the bristles. In this regard, an internal variable $\hat{\xi}$ is introduced which is the average bristle deflection. Hence, the friction force f features two state variables, and $f = f_{LM}(\hat{\xi}, X')$ is described as

$$f_{LM}(\hat{\xi}, X') = \delta_0 \hat{\xi} + \delta_1 \hat{\xi}' + \delta_2 X' \quad (6)$$

where δ_0 and δ_1 describe the stiffness and damping coefficients of the bristle, respectively. δ_2 represents the viscous part of the resistant force. $\hat{\xi}$ is the average bristle deflection, and the evolution of the average bristle deflection is governed by

$$\hat{\xi}' = X' \left[1 - \frac{\hat{\xi}}{\mathcal{G}(X')} \text{sgn}(X') \right] \quad (7)$$

where $\mathcal{G}(X') = \frac{N}{\delta_0} [\eta_c + \Delta\eta e^{-(X'/v_s)^\alpha}]$ dominates the Stribeck effect, v_s denotes the critical Sticbeck velocity, $\Delta\eta = \eta_s - \eta_c$, η_c describes the minimum level of the Coulomb friction, η_s denotes the level of the static friction and α is the parameter of slope to be designed ($\mathcal{G}(X')$ is referred to as the Gaussian friction model when $\alpha = 2$).

The Exponential friction force $f = f_{EM}(X')$ is introduced as

$$f_{EM}(X') = N[\eta_c + \Delta\eta e^{-\alpha|X'|}] \text{sgn}(X') \quad (8)$$

We introduce two state vectors in the extended phase spaces containing the internal state vector $\hat{\xi}$ to

allocate the system dynamics into state-space. For the capsule systems with the LM and the EM, respectively, the state vectors are defined as

$$S_{LM} := (y_1, y_2, y_3, y_4, y_5) \in \mathfrak{R}^{5 \times 1} := (\theta, \theta', X, X', \hat{\xi}) \in \mathfrak{R}^{5 \times 1}$$

$$S_{EM} := (y_1, y_2, y_3, y_4) \in \mathfrak{R}^{4 \times 1} := (\theta, \theta', X, X') \in \mathfrak{R}^{4 \times 1}$$

Decoupling Eqs. (4) and (5), and combining with Eqs. (6) and (8), a set of first-order differential equations in accordance with the defined state vectors above is yielded as

$$\begin{aligned} y_1' &= y_2 \\ y_2' &= \frac{1}{B} [(\lambda + 1)h\cos(\omega\tau) + (\lambda + 1)(\sin(y_1) - \rho y_1 - \nu y_2) - \sin(y_1)\cos(y_1)y_2^2 - Nf_1(y_4)\cos(y_1)] \\ y_3' &= y_4 \\ y_4' &= \frac{1}{B} [\cos(y_1)h\cos(\omega\tau) + \cos(y_1)(\sin(y_1) - \rho y_1 - \nu y_2) - \sin(y_1)y_2^2 - Nf_1(y_4)] \\ y_5' &= \Delta \end{aligned} \tag{9}$$

where $B = \lambda + 1 - \cos^2(y_1)$, and for the capsule system with LM, $f_1(y_4) = \delta_0 y_5 + \delta_1 y_5' + \delta_2 y_4$, $\Delta = y_4(1 - \frac{y_5}{\varphi(y_4)} \text{sgn}(y_4))$ and $\varphi(y_4) = \frac{N}{\delta_0} (\eta_c + \Delta \eta e^{-(y_4/v_s)^2})$; for the capsule system with EM, $f_1(y_4) = (\eta_c + \Delta \eta e^{-a|y_4|}) \text{sgn}(y_4)$ and $\Delta = 0$.

Remark 3: The additional state $\hat{\xi}$ in S_{LM} is the distinguishing factor that governs the evolution of the dynamic friction forces. However, there are limited reports in the literature on how $\hat{\xi}$ manipulates the dynamic frictional characteristics (e.g., drooping) of capsule systems during the presliding and the pure sliding phases. In this regard, the role of $\hat{\xi}$ will be studied elaborately in this paper.

2.3.3 Analysis of dynamic frictional limit

Fig. 4 depicts the microscopic elastic limits for the sticking, presliding and pure sliding phases. It is experimentally observed in the literature that the frictional dynamics act like springs at the sticking phase. A presliding displacement exists during the sticking phase that can be approximated through a linear representation of the static friction as shown in Fig. 4(b). Fig. 4(c) demonstrates the moment of a breakaway taking place when the threshold force is met, and at the meantime, the micro-connections are disrupted. Conventional studies on the friction-induced capsule dynamics have been reported using numerical analysis (Liu et al., 2013b, 2013a) or analytical analysis (H. Fang and Xu, 2011; Fang and Xu, 2012). In this paper, non-reversible characteristic of the friction dynamics for the static friction, the presliding and the pure sliding phases are studied analytically through the frictional limit, and the boundaries are identified.

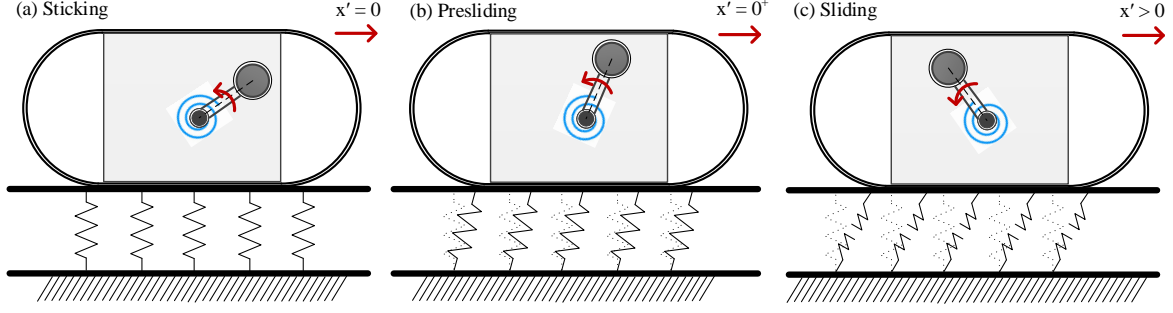


Fig. 4. Schematics of the microscopic elastic limit for the sticking, presliding and pure sliding phases.

From the friction models, it is noted that the friction force begins with strapping the contacting bodies by generating slipping motions relative to each other, and only microscopic deformations of the substrate occur at this stage. Also, these micro-connections are disrupted when the frictional limit is reached. In the quasi-static phase when no macroscopic sliding exists, $\varphi(X')$ in Eq. (7) indicates that the bristle deflection evolves proportionally with the internal state variable ξ and the friction force. The breakaway of bristles (i.e., the sign of ξ changes) occurs when $\xi = \varphi(X'(\tau))$ is satisfied. As a result, the maximum static friction force can be reached under the conditions of $X''(\tau) = 0$ and $\dot{\xi}' = 0$, and accordingly, we have

$$\varphi(X') = \frac{N}{\delta_0} \left[\eta_c + (\eta_s - \eta_c) e^{-(X'/v_s)^\alpha} \right] \quad (10)$$

where η_s denotes the maximum static friction during the quasi-static motion regime.

When the capsule moves with steady-state motion, the rate of deflections of the bristles is contained at zero (i.e., $\dot{\xi}' = 0$) and relative sliding motions occur between two bodies in contact. Therefore, the frictional dynamics are given as

$$f = \delta_0 \varphi(X') + \delta_2 X' = N \left[\eta_c + (\eta_s - \eta_c) e^{-(X'/v_s)^\alpha} \right] + \delta_2 X' \quad (11)$$

$$\frac{\partial f}{\partial X'} = -\alpha N \frac{X'^{\alpha-1}}{v_s^\alpha} (\eta_s - \eta_c) e^{-(X'/v_s)^\alpha} + \delta_2 \quad (12)$$

Comparing to the Stribeck velocity v_s , the first term on the right side of Eq. (12) is negligible by assuming that the motion of capsule is with sufficiently small or large average velocity. Therefore, it is plausible to make a supposition that, during the sliding regime, the average velocity has two offset values labelled as X'_l (lower velocity) and X'_h (higher velocity). For the velocity values $X'(\tau) \in (0, X'_l)$ and $X'(\tau) \in (X'_h, X'_{max})$ (X'_{max} denotes the maximum velocity that the capsule can obtain), the friction force is a monotonically increasing function of average velocity. On the other hand, for the velocity value $X'(\tau) \in (X'_l, X'_h)$, the friction force decreases monotonically. At the offset points $X'(\tau) = X'_l$ and $X'(\tau) = X'_h$, the slope of the friction curve becomes zero. These findings will be verified and demonstrated in the numerical analysis. The analytical values of X'_l and X'_h can be achieved by solving Eq. (12) and letting $\partial f / \partial X' = 0$, gives

$$-\alpha N \frac{X'^{\alpha-1}}{v_s^\alpha} (\eta_s - \eta_c) e^{-(X'/v_s)^\alpha} + \delta_2 = 0 \quad (13)$$

It is noted that the lower velocity value $X'(\tau) = X'_l$ should be sufficiently small as the velocity is

extremely low. Let $(X'/v_s)^\alpha = 0$, we have

$$X'_l = v_s \left[\frac{\delta_2 v_s}{\alpha N (\eta_s - \eta_c)} \right]^{1/(\alpha-1)} \quad (14)$$

On the other hand, for the higher velocity value $X'(\tau) = X'_h$, it is noted that X'_h stays in adjacency of the Stribeck velocity value v_s . Therefore, it can be obtained recursively as

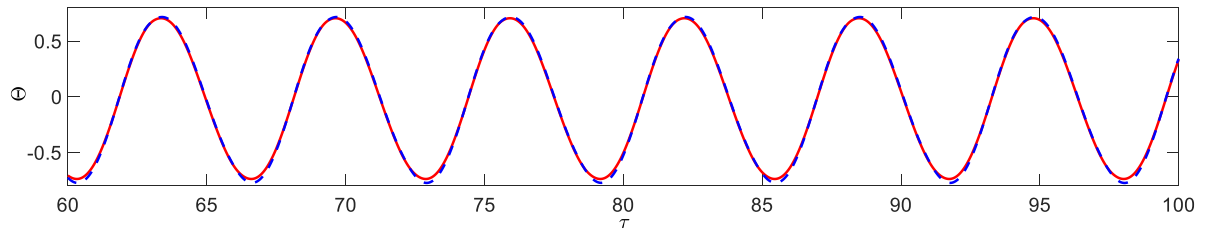
$$\left(\frac{X'_h}{v_s} \right)_{n+1} = \left\{ \ln \left[\left(\frac{\alpha N (\eta_s - \eta_c)}{\delta_2 v_s} \right)^{1/(\alpha-1)} \left(\frac{X'_h}{v_s} \right)_n \right] \right\}^{1/2} \quad (15)$$

3. Numerical analysis of the frictional interaction dynamics

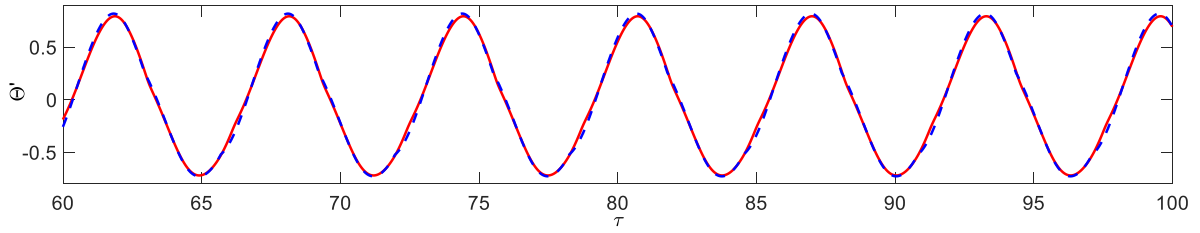
In this section, the interaction dynamic responses of the capsule models with the LM and the EM are first analysed to reveal the nonlinear friction characteristics. Subsequently, the effects of the control parameters are studied closely to identify the parameter dependence and the qualitative variation laws in capsule dynamics. The Gaussian friction model is adopted in this study as the exponential term in LM, i.e., $\alpha = 2$. The rationality of the parameters chosen in this section is described as follows: parameter values of the LM and EM are configured from the dynamic friction studies in literature as reported in (Chatterjee, 2007; Olsson et al., 1998; Saha et al., 2015) ($\delta_0 = 100$, $\delta_1 = 10$, $\delta_2 = 0$, $N = 1$, $\eta_c = 0.15$, $\eta_s = 0.45$, $v_s = 0.1$ and $\alpha = 10$); the control parameter values and the initial conditions of state variables are selected based on our previous (Liu et al., 2015) and ongoing works on identification of the qualitative variation laws induced by the control parameters ($y_1(0) = \pi/3$, $y_2(0) = 0$, $y_3(0) = 0$, $y_4(0) = 0$ and $y_5(0) = 0.0026$). The numerical studies in this section are based on the system dynamics in Eq. (9).

3.1 The friction-induced vibrations

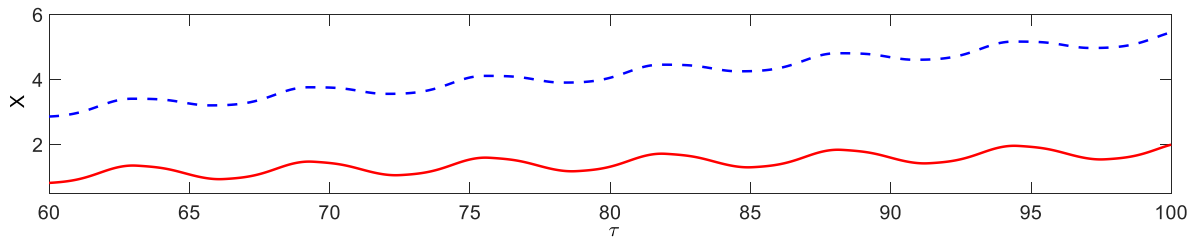
The time domain dynamic responses of the capsule systems with the EM and the LM are portrayed in Figs. 5 and 6, respectively. It is noted that the negative slope characteristic is observed in the figures which guarantees the stability of the system. The EM is able to describe the Stribeck effect, while it is inherently a static model of the friction which does not interpret the hysteretic behaviour. The LM falls into the categories of dynamic models and is capable of predicting the hysteretic loops. The friction-induced vibrational responses with the EM and the LM are depicted in Fig. 5. The capsule with the LM exhibits similar variation patterns to the one with the EM in angular displacement θ , angular velocity θ' , capsule displacement X and capsule velocity X' . It is noted that the main difference lies into the transitions between the sticking regime and the pure sliding regime. As depicted in Fig. 5(d), the relative velocity does not drop down to zero completely during the sticking regime, this is affected by the friction's hysteretic characteristic during the presliding regime. It is noted that without the hysteretic behaviour in the EM in the presliding regime, the sticking regime exerts a greater influence on the EM than that on the LM, which leads fluctuations of the capsule velocity around zero. It is also observed from Figs. 5(c) and 5(d) that higher velocity and larger displacement of the systems are obtained for the capsule with the EM than that with the LM, the reason behind is that capsule with the EM avoids the energy loss in the hysteretic loop.



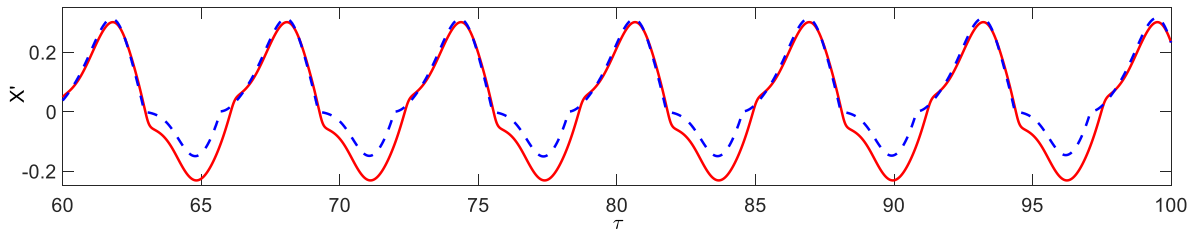
(a) The angular displacements θ



(b) The angular velocities θ'

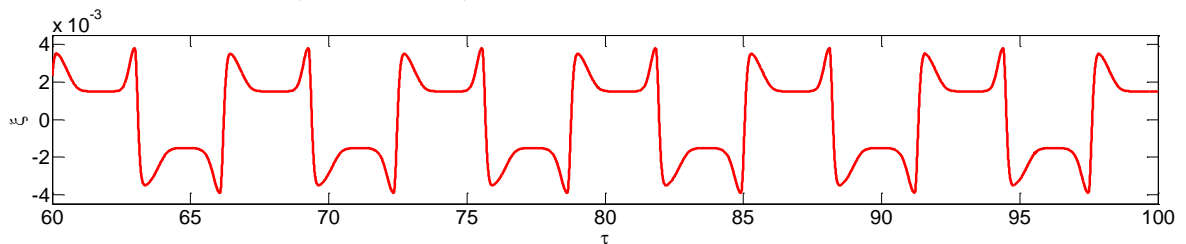


(c) The capsule displacements X

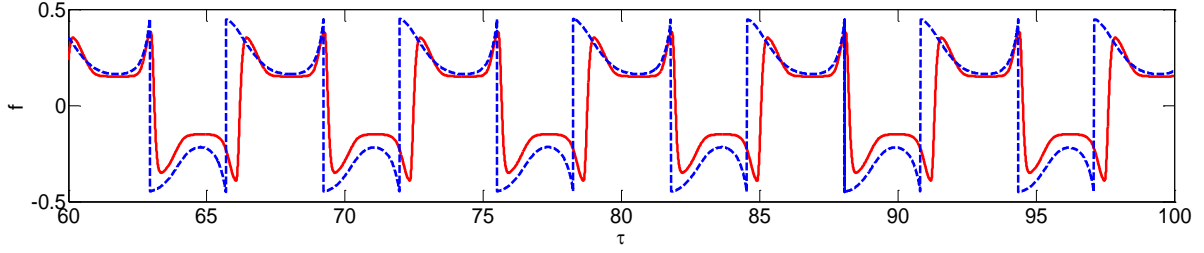


(d) The capsule velocity X'

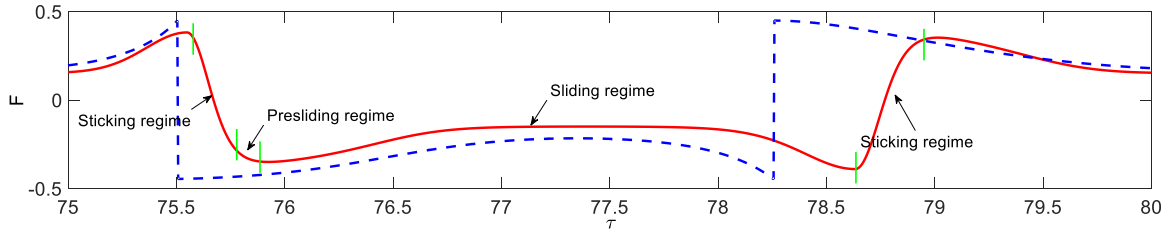
Fig. 5. Friction-induced vibrational response of the system with the EM (blue dashed lines) and system with the LM (red solid lines), obtained for $\lambda = 2.5$, $\rho = 2.0$ and $v = 1.0$.



(a) The internal state variable ξ



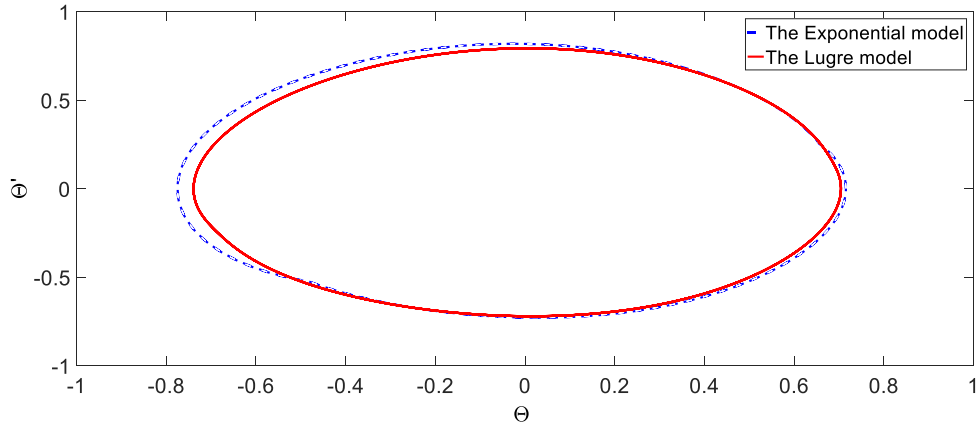
(b) The friction forces f



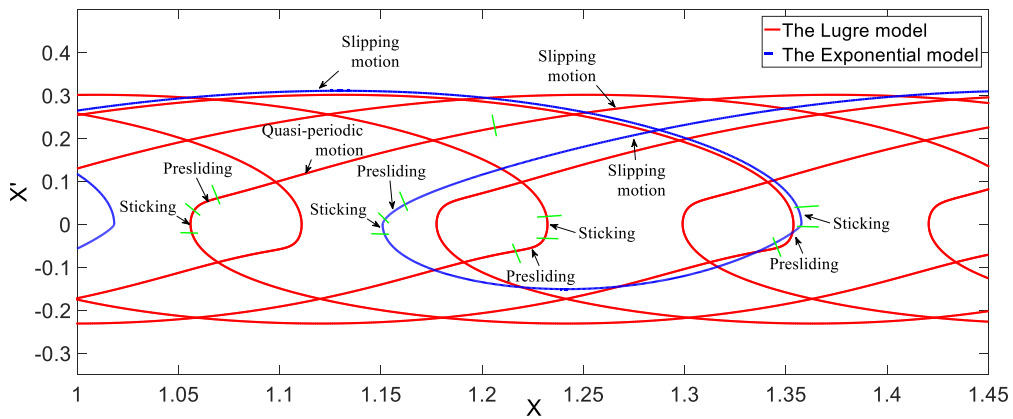
(c) Enlarged friction forces F

Fig. 6. Friction-induced vibrational responses of the system with the EM (blue dashed lines) and the system with the LM (red solid lines), obtained for $\lambda = 2.5$, $\rho = 2.0$ and $v = 1.0$.

From, Fig. 6, it is observed that the dynamic responses of the internal state variable $\hat{\xi}$ and friction force f have a similar variation law. This indicates that $\hat{\xi}$ governs the evolution of f . Specifically, during the onset of the sticking regime, $\hat{\xi}$ decreases significantly from a certain level and increases monotonically until the same level in the opposite direction. The value of the average bristle deflection $\hat{\xi}$ changes in both pure sliding and presliding regimes that it firstly decreases in the AS and then augments in the DS in a periodic pattern. This is affected by function $g(X')$ which dominates the evolution of the internal state variable $\hat{\xi}$. Figs. 6(b) and 6(c) demonstrates sharp declines of the friction force and then indicates the onsets of the sticking regime. Subsequently, the friction rises monotonically during the sticking regime until it reaches the boundary of the static friction. Therefore, the roles of the state variable $\hat{\xi}$ are be concluded as: it manipulates the hysteretic behaviour in the presliding and pure sliding regimes, and the characteristic of drooping during the pure sliding regime. Interestingly, these findings in friction-induced vibrations coincide with the results reported in (Astrom and Canudas-De-Wit, 2008; Chatterjee, 2007; Saha et al., 2015), in which several fully-actuated systems are studies. The capsule systems considered in this paper are underactuated, and the friction has an indirect mapping to the input, which, in turn, verifies the results presented here.



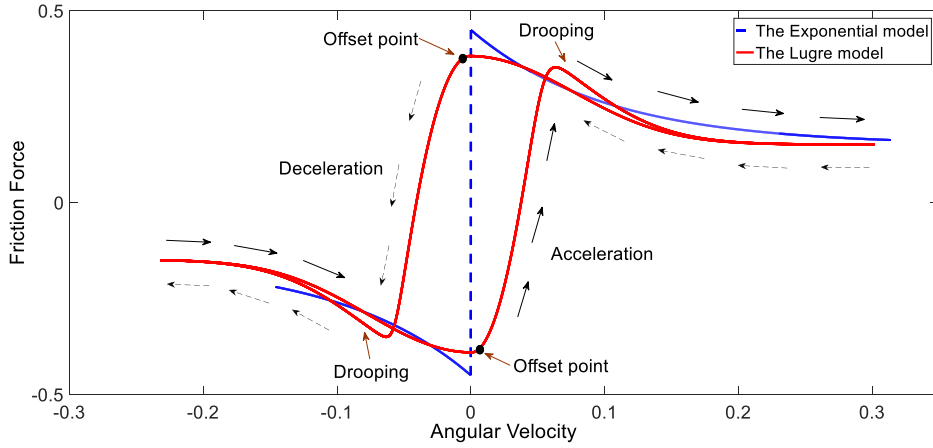
(a) The pendulum subsystem



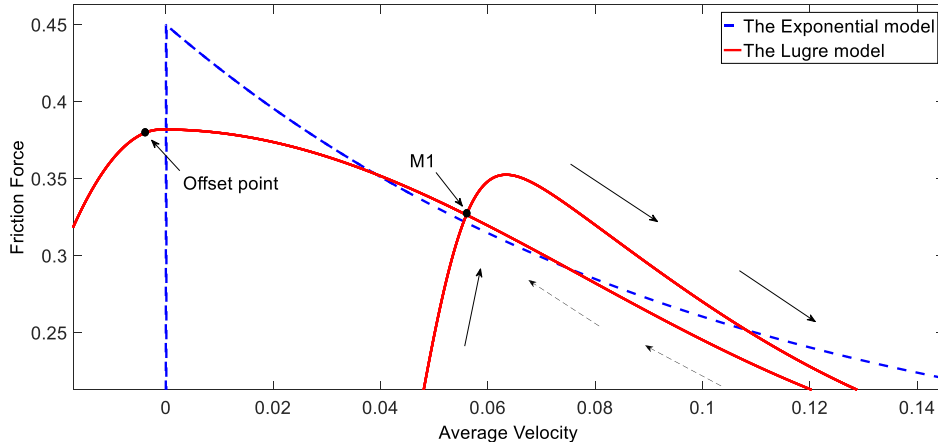
(b) The capsule subsystem

Fig. 7. Phase plane trajectories of the capsule systems with the EM (blue dashed lines) and the LM (red solid lines), obtained for $\lambda = 2.5$, $\rho = 2.0$ and $\nu = 1.0$.

The phase plane trajectory of the pendulum subsystem (θ and θ') and the capsule subsystem (X and X') are portrayed in Fig. 7. A relatively larger limit cycle is observed for the capsule with the EM than that with the LM. The reason behind is the energy loss resulted from the hysteretic behaviour of the frictional dynamics with the LM. Several steps are also observed in Fig. 7(a) and 7(b) when the value of relative velocity pass through zero, and accordingly, the frictional dynamics becomes quasi-static in this phase. It is also observed that slight discontinuities exist associated with imperfect overlaps between the beginning and the end of the limit cycle. It is noted that the dynamics shown in Fig.7 are not strictly periodic. However, they are constrained to reside within some finite boundaries. As a result, dynamic responses in this regime are classified into quasi-periodic motions, and this is due to the hysteretic characteristic of the friction.



(a) Friction curves



(b) Enlarged friction curves

Fig. 8. Friction forces for the capsule systems with the EM (blue dashed lines) and the LM (red solid lines) show the friction characteristics near zero velocity, obtained for $\lambda = 2.5$, $\rho = 2.0$ and $v = 1.0$.

As shown in Fig.8, the hysteretic loops are characterized as the friction which is a function of the average velocity of the capsule system. The loop (in blue dash line) for the capsule system with the EM does not demonstrate the hysteretic behaviour. This cross-validates the numerical results in Figs. 5 and 6 that the system with the EM performs oscillations with relatively higher frequency than that with the LM. Besides, a lower maximum friction force is obtained for the system with the LM than that with the EM, with same set of parameter values, e.g., the stiction force level η_s , the Coulomb friction level η_c , and the Stribeck velocity v_s . The reason behind is the dimension reduction of the limit cycle for the capsule system with the LM. Moreover, the arrow flows as shown in Fig. 8 depict the variations of the friction in accordance with the changes in velocity for the capsule system with the LM. For backward and forward motions, it is also noted that the friction force has relatively smaller value in the DS than that in the AS during the pure sliding regime. As a result, a clockwise hysteretic loop takes place during the pure sliding regime. While the trend is completely different near the zero velocity: the friction force in

the AS is smaller than that in the DS. The DS and the AS are portrayed with arrows that are in accordance with the decreasing and increasing of the relative velocity of the capsule, respectively. It is apparently observed that the hysteretic curves have offset points near the regime of zero when the friction changes from small displacement in the AS to massive displacement in the DS, respectively.

During the forward motion stage of the capsule systems, M_1 is an identified boundary point between the pure sliding and presliding regimes. Precisely, the capsule system escapes from the presliding regime and then accesses the pure sliding regime at M_1 . Meanwhile, the friction firstly rises to a certain level within the boundary of the maximal value of the Exponential friction, and then declines monotonously in accordance with the augmenting average velocity, and finally terminals and overlaps with the DS. Interestingly, the trajectories of the capsule system with the EM and with the LM almost coincide with each other around M_1 . It is also found that between M_1 and the terminal point, the friction force for the DS is always smaller than that for the AS. The trend between M_1 and the offset point is reversed.

3.2 Influence of the control parameters

The solutions and their stabilities play a vital role in the system responses. A proper tuning of the control parameters will improve the system performance and avoid undesirable responses. The capsule system moves from the origin, so its average velocity is bounded and can reveal the qualitative changes in the system responses. The average velocity X' is plotted as a function of mass ratio λ to reveal the parameter dependence.

In this subsection, the mass ratio λ is considered as the branching control parameter. The numerical results are presented in Fig. 9, the average velocities of the capsule systems with the EM (blue dotted line) and the LM (red dotted line) are illustrated and projected as functions of λ . The average velocity is defined as the average (forward) progression of the capsule systems per period of excitation.

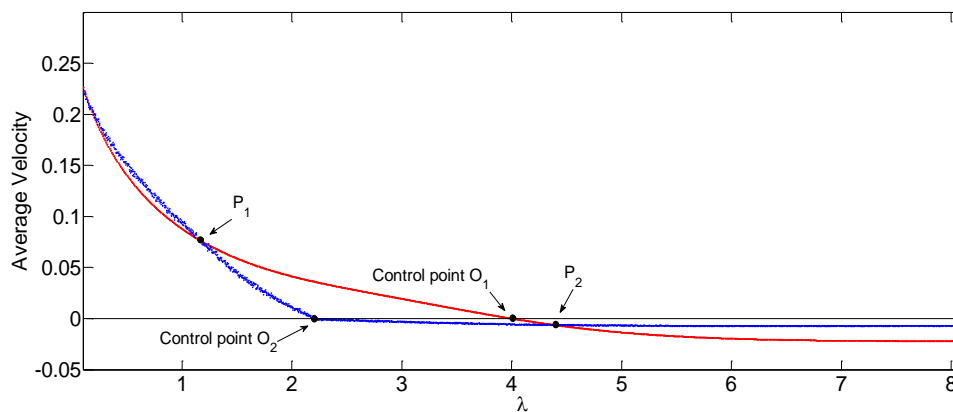


Fig. 9. Dynamic responses of the capsule systems with the EM (blue dotted) and the LM (red dotted) constructed under variation of the mass ratio λ , obtained for $h = 1.8$, $\omega = 1.0$, $\rho = 4.0$ and $v = 1.2$.

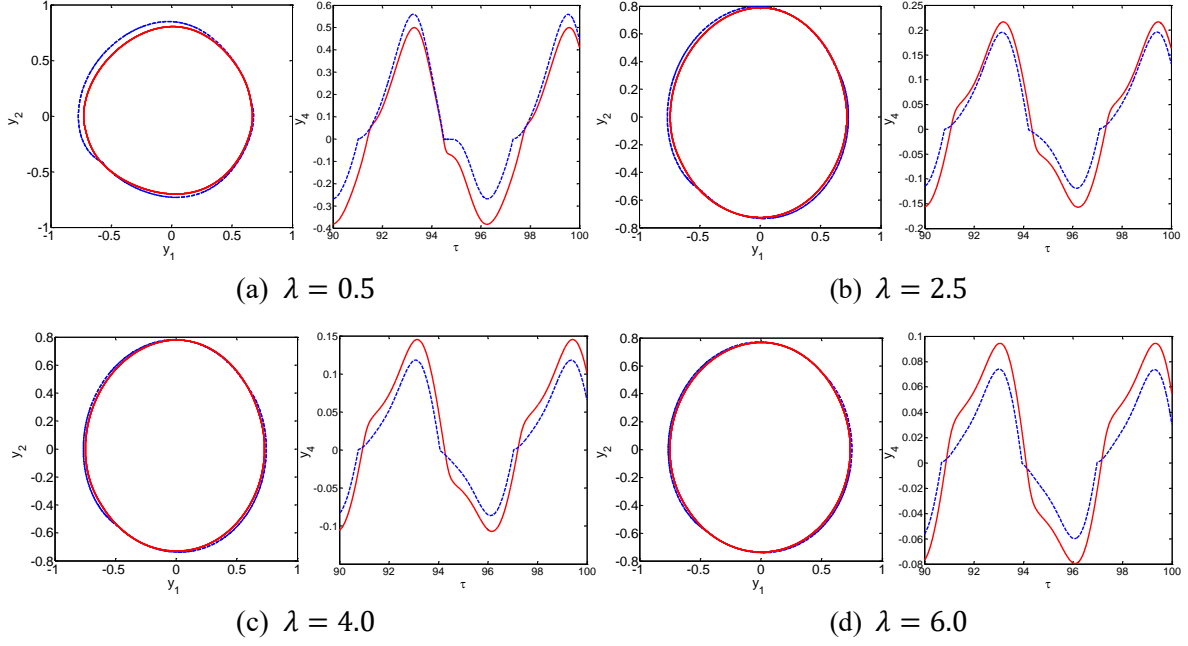
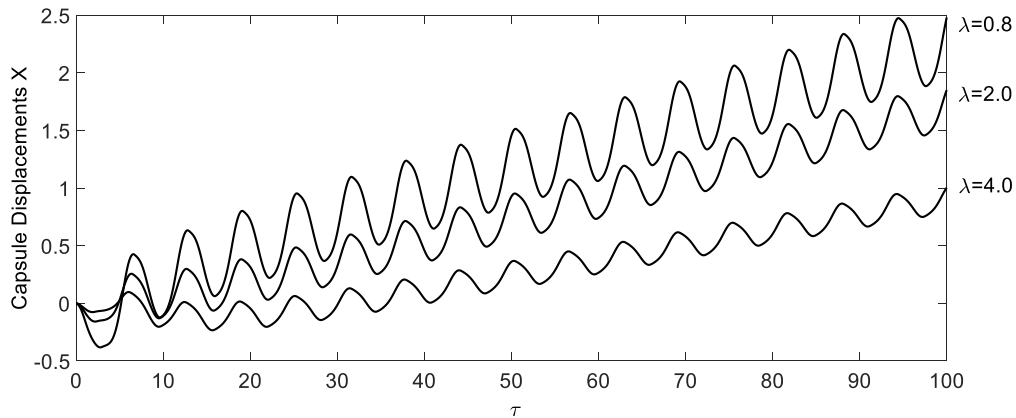


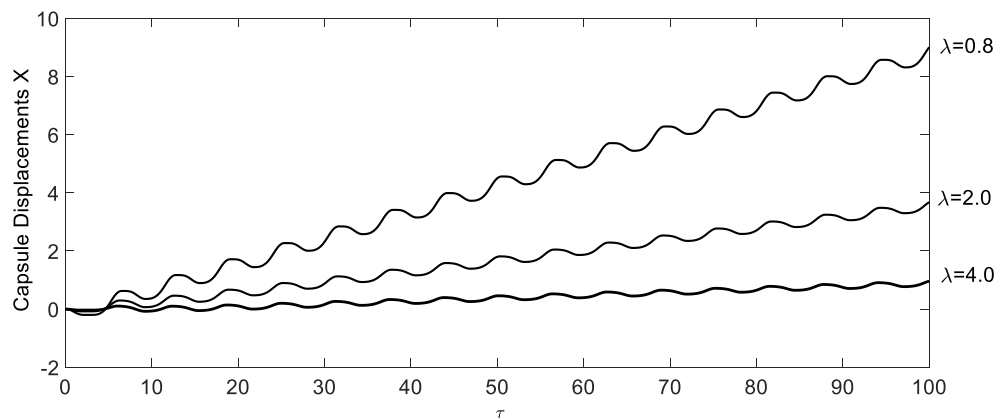
Fig. 10. Phase domain trajectories for the pendulum subsystem (y_1 and y_2) and time domain trajectories for the capsule subsystem (progressive velocity y_4), with the LM (red solid lines) and the EM (blue dashed lines), obtained for $h = 1.8$, $\omega = 1.0$, $\rho = 4.0$ and $v = 1.2$.

From Fig. 9, it is noted that periodic system responses are predicted for λ considered in this paper. Both curves demonstrate the negative slope characteristic with different magnitudes: the capsule system with the EM has a relatively larger negative slope than that with the LM. From the numerical results, we can also observe that with both friction models, the average velocities decrease monotonically with the increasing of λ for $\lambda \in [0.01, 8.1]$. Boundary points at P_1 ($\lambda = 1.18$) and P_2 ($\lambda = 4.36$) are identified that separate the performances of capsule systems. Specifically, the capsule with the EM obtains a relatively higher velocity than that with the LM before the boundary point P_1 . For the mass ratio between points P_1 and P_2 $\lambda \in [1.18, 4.36]$, the trend is reversed: the average velocity of the capsule with the EM is lower than that with the LM. However, beyond point P_2 for $\lambda \in [4.36, 8.1]$, the capsule with the EM overtakes that with the LM again near the zero velocity while in the negative direction. As can be observed in Fig. 9, the capsule moves with positive velocities for $\lambda \leq 4.0$ and $\lambda \leq 2.2$ with the LM and the EM, respectively. On the other hand, the capsule moves with negative speeds are recorded for $\lambda \in [2.2, 8.1]$ with the EM and for $\lambda \in [4.0, 8.1]$ with the LM. The time domain trajectory of the capsule velocity and phase domain trajectory of the driving pendulum are portrayed in Fig. 10. It is recorded that with both the LM and EM, the capsules move with larger positive velocities in each period of excitation for $\lambda \leq 4.0$ and $\lambda \leq 2.2$. And subsequently, the magnitude of velocity declines dramatically in the positive direction as λ increases. As a result, the average speeds of the capsules drop down below zero. Therefore, the average capsule velocity can be controlled by appropriate tuning of the mass ratio λ around the identified control point O_1 at $\lambda = 4.0$ for the system with the LM, and around the identified control point O_2 at $\lambda = 2.2$ for the system with the EM.

Comparison of the travel distance of the capsule systems under the variation of λ is shown in Fig. 11. For the capsule systems with the LM and the EM, it is clearly observed that both the travelling distance decrease monotonically in accordance with the augmentation of λ . Similarly, the amplitude of the displacement curves reduces as λ increases. On the other hand, towards an increasing mass ratio, capsule travelling distance with the EM exerts a more significant decline rate than that of the system with the LM. It can be concluded that this is due to the difference in the negative slopes of the average velocity curves.



(a) Capsule system with the LM



(b) Capsule system with the EM

Fig. 11. Time histories of the capsule displacements under the varying mass ratio ($\lambda = 0.8, 2.0$ and 4.0), obtained for $h = 1.8$, $\omega = 1.0$, $\rho = 4.0$ and $v = 1.2$.

4. Conclusions

The motion of the vibro-driven capsule systems relies on the inherently nonlinear effects of the dynamic frictions. The nonlinear friction forces can trigger dynamic interactions between the systems and the substrate in contact. Towards the capsule systems, the dynamic frictional characteristics have been studied in this paper. The main difference between the friction models exists in the transitions between the sticking and the pure sliding regimes. It is found that the hysteretic characteristic has a significant influence on the relative velocity during the presliding regime, and it does not drop down to zero entirely during the sticking regime. The role of $\hat{\xi}$ in dominating the drooping characteristic of the friction

during the pure sliding regime, and the hysteretic behaviours during the presliding and pure sliding regimes have been precisely discussed. The dependence on multi-control parameters has been investigated. It is also demonstrated that the interaction models predict periodic responses of the system dynamics. Average motion velocity decreases monotonously along with the increasing of the mass ratio λ and, in turn, a control action can be applied by appropriate tuning of the multi-control parameters. The studies on the capsule dynamics also provide the desirability of the LM than the EM during most of the evaluations of the system performance. The performance evaluations used for comparison of the friction models contain the capabilities of seizing the frictional characteristics that have been observed in the experiments, the energy requirements, and quenching of the vibrations induced by the friction.

Funding: This work was partially supported by the National Natural Science Foundation of China (grant numbers 61803396), European Commission Marie Skłodowska-Curie SMOOTH (Smart robots for fire-fighting) project (H2020-MSCA-RISE-2016-734875) and Royal Society International Exchanges Scheme (Adaptive Learning Control of a Cardiovascular Robot using Expert Surgeon Techniques) project (IE151224).

References

- Al-Bender, F., Swevers, J., 2008. Characterization of friction force dynamics. *IEEE Control Syst.* 28, 64–81.
- Alexander, R., Dimery, N.J., Ker, R.F., 1985. Elastic structures in the back and their role in galloping in some mammals. *J. Zool.* 207, 467–482.
- Armstrong-Hélouvy, B., Dupont, P., De Wit, C.C., 1994. A survey of models, analysis tools and compensation methods for the control of machines with friction. *Automatica* 30, 1083–1138. [https://doi.org/10.1016/0005-1098\(94\)90209-7](https://doi.org/10.1016/0005-1098(94)90209-7)
- Astrom, K.J., Canudas-De-Wit, C., 2008. Revisiting the LuGre friction model. *Control Syst. IEEE* 28, 101–114.
- Becker, T.C., Mahin, S.A., 2013. Effect of support rotation on triple friction pendulum bearing behavior. *Earthq. Eng. Struct. Dyn.* 42, 1731–1748.
- Biswas, S., Chatterjee, A., 2014. A reduced-order model from high-dimensional frictional hysteresis, in: *Proceedings of the Royal Society of London A: Mathematical, Physical and Engineering Sciences*. The Royal Society, p. 20130817.
- Bolotnik, N.N., Figurina, T.Y., 2008. Optimal control of the rectilinear motion of a rigid body on a rough plane by means of the motion of two internal masses. *J. Appl. Math. Mech.* 72, 126–135.
- Casini, P., Giannini, O., Vestroni, F., 2012. Persistent and ghost nonlinear normal modes in the forced response of non-smooth systems. *Phys. Nonlinear Phenom.* 241, 2058–2067.
- Chatterjee, S., 2007. Non-linear control of friction-induced self-excited vibration. *Int. J. Non-Linear Mech.* 42, 459–469. <https://doi.org/10.1016/j.ijnonlinmec.2007.01.015>
- Chernous'ko, F.L., 2002. The optimum rectilinear motion of a two-mass system. *J. Appl. Math. Mech.* 66, 1–7.
- Chernous'ko, F.L., 2011. Analysis and optimization of the rectilinear motion of a two-body system. *J. Appl. Math. Mech.* 75, 493–500.
- Chowdhury, M.A., Helali, M., 2008. The effect of amplitude of vibration on the coefficient of friction for different materials. *Tribol. Int.* 41, 307–314. <https://doi.org/10.1016/j.triboint.2007.08.005>
- De Wit, C.C., Olsson, H., Astrom, K.J., Lischinsky, P., 1995. A new model for control of systems with friction. *Autom. Control IEEE Trans. On* 40, 419–425.

- Dimery, N.J., Alexander, R., Ker, R.F., 1986. Elastic extension of leg tendons in the locomotion of horses (*Equus caballus*). *J. Zool.* 210, 415–425.
- Fang, H., Xu, J., 2013. Stick-Slip Effect in a Vibration-Driven System With Dry Friction: Sliding Bifurcations and Optimization. *J. Appl. Mech.* 81, 051001–051001. <https://doi.org/10.1115/1.4025747>
- Fang, H., Xu, J., 2011. Dynamics of a mobile system with an internal acceleration-controlled mass in a resistive medium. *J. Sound Vib.* 330, 4002–4018. <https://doi.org/10.1016/j.jsv.2011.03.010>
- Fang, H.-B., Xu, J., 2012. Controlled motion of a two-module vibration-driven system induced by internal acceleration-controlled masses. *Arch. Appl. Mech.* 82, 461–477.
- Fang, H.B., Xu, J., 2011. Dynamic analysis and optimization of a three-phase control mode of a mobile system with an internal mass. *J. Vib. Control* 17, 19–26.
- Giannini, O., Casini, P., Vestroni, F., 2011. Experimental evidence of bifurcating nonlinear normal modes in piecewise linear systems. *Nonlinear Dyn.* 63, 655–666.
- H. B. Fang, J.X., 2010. Dynamic Analysis and Optimization of a Three-phase Control Mode of a Mobile System with an Internal Mass. *J. Vib. Control - J VIB CONTROL* 16. <https://doi.org/10.1177/1077546309345631>
- Hetzler, H., Schwarzer, D., Seemann, W., 2007. Analytical investigation of steady-state stability and Hopf-bifurcations occurring in sliding friction oscillators with application to low-frequency disc brake noise. *Commun. Nonlinear Sci. Numer. Simul.* 12, 83–99.
- Huda, M.N., Yu, H., 2015. Trajectory tracking control of an underactuated capsulobot. *Auton. Robots* 39, 183–198. <https://doi.org/10.1007/s10514-015-9434-3>
- Kim, J.-S., Sung, I.-H., Kim, Y.-T., Kim, D.-E., Jang, Y.-H., 2007. Analytical model development for the prediction of the frictional resistance of a capsule endoscope inside an intestine. *Proc. Inst. Mech. Eng. [H]* 221, 837–845. <https://doi.org/10.1243/09544119JEIM173>
- Li, H., Furuta, K., Chernousko, F.L., 2006. Motion generation of the capsulobot using internal force and static friction, in: *Decision and Control, 2006 45th IEEE Conference on*. pp. 6575–6580.
- Liu, P., Yu, H., Cang, S., 2018a. Optimized adaptive tracking control for an underactuated vibro-driven capsule system. *Nonlinear Dyn.* 1–15.
- Liu, P., Yu, H., Cang, S., 2018b. Trajectory Synthesis and Optimization of an Underactuated Microrobotic System with Dynamic Constraints and Couplings. *Int. J. Control Autom. Syst.* 1–11.
- Liu, P., Yu, H., Cang, S., 2018c. On the dynamics of a vibro-driven capsule system. *Arch. Appl. Mech.* 1–21.
- Liu, P., Yu, H., Cang, S., 2017. Geometric analysis-based trajectory planning and control for underactuated capsule systems with viscoelastic property. *Trans. Inst. Meas. Control* 0142331217708833. <https://doi.org/10.1177/0142331217708833>
- Liu, P., Yu, H., Cang, S., 2016. Modelling and dynamic analysis of underactuated capsule systems with friction-induced hysteresis, in: *Intelligent Robots and Systems (IROS), 2016 IEEE/RSJ International Conference on*. IEEE, pp. 549–554.
- Liu, P., Yu, H., Cang, S., 2015. On periodically pendulum-driven systems for underactuated locomotion: A viscoelastic jointed model, in: *Automation and Computing (ICAC), 2015 21st International Conference on*.
- Liu, P., Yu, H., Cang, S., 2014. Modelling and control of an elastically joint-actuated cart-pole underactuated system, in: *Automation and Computing (ICAC), 2014 20th International Conference on*. IEEE, pp. 26–31.
- Liu, Y., Pavlovskaja, E., Hendry, D., Wiercigroch, M., 2013a. Vibro-impact responses of capsule system with various friction models. *Int. J. Mech. Sci.* 72, 39–54.
- Liu, Y., Wiercigroch, M., Pavlovskaja, E., Yu, H., 2013b. Modelling of a vibro-impact capsule system. *Int. J. Mech. Sci.* 66, 2–11. <https://doi.org/10.1016/j.ijmecsci.2012.09.012>
- McMahon, T.A., 1985. The role of compliance in mammalian running gaits. *J. Exp. Biol.* 115, 263–282.

- McMillan, A.J., 1997. A NON-LINEAR FRICTION MODEL FOR SELF-EXCITED VIBRATIONS. *J. Sound Vib.* 205, 323–335. <https://doi.org/10.1006/jsvi.1997.1053>
- Neis, P.D., De Baets, P., Ost, W., Delgado, Y.P., Loccufier, M., Al-Bender, F., Ferreira, N.F., Lorini, F.J., 2011. Investigation of the dynamic response in a dry friction process using a rotating stick–slip tester. *Wear* 271, 2640–2650.
- Olsson, H., Åström, K.J., Canudas de Wit, C., Gäfvert, M., Lischinsky, P., 1998. Friction Models and Friction Compensation. *Eur. J. Control* 4, 176–195. [https://doi.org/10.1016/S0947-3580\(98\)70113-X](https://doi.org/10.1016/S0947-3580(98)70113-X)
- Outirba, B., Hendrick, P., 2014. Experimental Testing of Carbon Brush Seals for Aero Engines Bearing Chambers, in: *ASME Turbo Expo 2014: Turbine Technical Conference and Exposition*. American Society of Mechanical Engineers, p. V05CT16A017–V05CT16A017.
- Saha, A., Wahi, P., Wiercigroch, M., Stefański, A., 2015. A modified LuGre friction model for an accurate prediction of friction force in the pure sliding regime. *Int. J. Non-Linear Mech.*
- Stefański, A., Wojewoda, J., Wiercigroch, M., Kapitaniak, T., 2006. Regular and chaotic oscillations of friction force. *Proc. Inst. Mech. Eng. Part C J. Mech. Eng. Sci.* 220, 273–284.
- Wojewoda, J., Stefański, A., Wiercigroch, M., Kapitaniak, T., 2008. Hysteretic effects of dry friction: modelling and experimental studies. *Philos. Trans. R. Soc. Lond. Math. Phys. Eng. Sci.* 366, 747–765.
- Zhan, X., Xu, J., 2015. Locomotion analysis of a vibration-driven system with three acceleration-controlled internal masses. *Adv. Mech. Eng.* 7, 1687814015573766.
- Zhang, C., Liu, H., Li, H., 2014a. Experimental investigation of intestinal frictional resistance in the starting process of the capsule robot. *Tribol. Int.* 70, 11–17. <https://doi.org/10.1016/j.triboint.2013.09.019>
- Zhang, C., Liu, H., Li, H., 2014b. Modeling of Frictional Resistance of a Capsule Robot Moving in the Intestine at a Constant Velocity. *Tribol. Lett.* 53, 71–78. <https://doi.org/10.1007/s11249-013-0244-5>
- Zhang, C., Liu, H., Tan, R., Li, H., 2012. Modeling of Velocity-dependent Frictional Resistance of a Capsule Robot Inside an Intestine. *Tribol. Lett.* 47, 295–301. <https://doi.org/10.1007/s11249-012-9980-1>